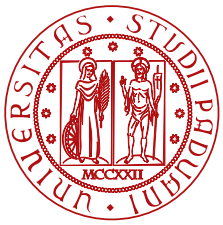

UNIVERSITÀ
DEGLI STUDI
DI PADOVA

DIPARTIMENTO
DI INGEGNERIA
DELL'INFORMAZIONE

DEPARTMENT OF INFORMATION ENGINEERING

BACHELOR'S DEGREE IN INFORMATION ENGINEERING

Interconnected lightsails for space exploration

Supervisor
Prof. Leonardo Badia

Candidate
Riccardo Dal Maschio

ACADEMIC YEAR 2023-2024

Graduation date 19/07/2024

Thesis. Antithesis. Synthesis

Abstract

The scope of this thesis is to explore the possible development of a swarm of interconnected lightsails for efficient and scalable space exploration. We focus on the comprehensive design and analysis of a nanosatellite architecture that relies on photonic thrusters (lightsail), alongside sophisticated laser communication systems tailored to ensure a reliable and efficient data transfer.

The analysis of different propulsion methods suggests that the best choice for such a mission is the use of the lightsail technology together with a lightweight payload based on the CubeSat architecture.

Additionally, this study investigates the integration of an optical communication system for long-distance space transmission, based on the existing technologies borrowed from the LCRD (Laser Communication Relay Demonstration) and LLCD (Lunar Laser Communication Demonstration) missions. Referring to these technologies, the thesis will examine the available modulation schemes and, via the exploitation of link budget computations, the maximum distances at which the probes have to be set apart is computed. Based on the results obtained, a preferred topology is recommended to ensure reliable communication between the satellites. Given that multiple probes within the swarm may fail during exploration, several redundancies and safeguards have been implemented to maintain the minimal operational performance of the swarm. Moreover, the thesis proposes some future innovations that could be adapted to improve the operations of the swarm and increase the reliability of the communication systems and of the lightsail architecture.

Abstract - Italiano

Lo scopo di questa tesi è quello di approfondire la possibilità di sviluppare uno sciame di vele solari interconesse per un'esplorazione spaziale efficente e scalabile. Il seguente lavoro si concentra sulla completa progettazione ed analisi dell'architettura di nanosatelliti che si baserà su propulsori fotonici (vele solari), affiancati da soffisticati sistemi di comunicazione laser progettati per garantire un trasferimento dei dati affidabile ed efficiente.

L'analisi dei diversi metodi di propulsione dimostrerà che la scelta migliore per una tale missione è l'utilizzo della tecnologia delle vele solari in combinazione con un *payload* leggero basato sull'architettura CubeSat.

Inoltre, questo studio prevede l'integrazione di un sistema di comunicazione ottico per la trasmissione a lunga distanza, questo si baserà sulle tecnologie esistenti dalle missioni LCRD (Laser Communication Relay Demonstration) e LLCD (Lunar Laser Communication Demonstration). Facendo riferimento alle tecnologie sopra citate, la tesi esaminerà gli schemi di modulazione disponibili e, tramite il calcolo del *link budget*, calcolerà le distanze massime a cui le sonde devono essere posizionate. In base ai risultati ottenuti, viene dunque raccomandata una particolare topologia per garantire un'affidabile comunicazione tra i vari satelliti.

Dato che più sonde all'interno dello sciame possono guastarsi durante l'esplorazione, sono state implementate diverse ridondanze e margini al fine di poter sempre mantenere le minime prestazioni dello sciame.

Inoltre, la tesi propone alcune future innovazioni che potrebbero essere adottate per migliorare le operazioni dello sciame e aumentare l'affidabilità dei sistemi di comunicazione e dell'architettura delle vele solari.

Contents

List of Figures

Acronyms

ARC Ames Research Centre. 17

AU Astronomical Unit. 11, 29, 32

BER Bit Error Rate. 24, 26–32

bps bits per second. 17, 20, 21

COTS Commercial Off-The-Shelf. 10, 18

DC Direct Current. 39

DPSK Differential Phase Shift Keing. ix, x, xv, 20, 21, 24, 26–28, 30–35, 39, 41, 42, 45

DSN Deep Space Network. 15

GEO Geostationary Orbit. 20

GSFC Goddard Space Flight Center. 18

HDD Hard Disk Drive. 36

ILLUMA-T Integrated Laser Communications Relay Demonstration Low Earth Orbit User Modem and Amplifier Terminal. 19

ISS International Space Station. 19

JPL Jet Propulsion Laboratory. 18

LADEE Lunar Atmosphere and Dust Environment Explorer. 17

LCRD Laser Communication Relay Demonstration. v, xiv, 2, 18–21, 24, 25, 35, 41

LL Lincoln Laboratory. 18, 21

LLCD Lunar Laser Communication Demonstration. v, xi, 2, 16, 17, 20, 24, 25, 41

LLGT Lunar Lasercom Ground Terminal. 17

LLOC Lunar Lasercom Operational Centre. 17

LLST Lunar Lasercom Space Terminal. 17

LMOC LCRD Mission Operations Center. 19

LOS Line of Sight. 7

MIT Massachussets Institute of Techonology. 18, 21

OGS-1 Optical Ground Station 1. 20

OGS-2 Optical Ground Station 2. 20

PPM Pulse Position Modulation. ix, x, xv, 20, 21, 24, 26–30, 32–35, 39, 41–43

RF Radio Frequency. 2, 15, 18

SNR Signal to Noise Ratio. 25–28, 30, 31

SSD Solid State Drive. 36

w.r.t. With respect to. 9, 18

Nomenclature

$\dot{m}$	Mass consumption rate [kg/s]
λ	Wavelength [m]
Ω_A	Solid angle [sr]
a_{Ch}	Attenuation of the channel
B_0	Minimum bandwidth [Hz]
c	Speed of light [m/s]
d	Distance [m]
D_r	Directivity of the receiver
D_t	Directivity of the transmitter
F	Noise figure
f	Frequency [Hz]
h	Planck's constant [Js^{-1}]
I_0	Irradiance [W/m^2]
k	Boltzmann constant [j/K]
L	Number of symbols in the PPM modulation
L_{Ch}	Path loss
M	Number of symbols in the DPSK modulation
P	Pressure [Pa]
p	Momentum [kg m/s]

P_b Bit error probability

P_{T_x} Transmitted power [W]

$Q(x)$ Q-function, the tail distribution function of the standard normal distribution

$Q^{-1}(x)$ Inverse Q-function

T_0 Room temperature (290 K)

T_w Time required to send a word [s]

T_{bit} Time required to send each bit [s]

$T_{eff,Rc}$ Effective noise temperature at the receiver [K]

U Energy of photon [J]

V_{ex} Exhaust velocity [m/s]

A Area [m^2] or Absorbance

B Bandwidth [Hz]

R Reflectance

Chapter 1

Introduction

Space exploration has always been characterized by extremely high costs and technical limitations. For this reason, the idea of developing a lightweight nanosatellite capable of reducing the launch costs and being driven beyond the limits of the solar system holds great potential for revolutionizing deep-space exploration [1].

Because of the gigantic distances that a deep space exploratory probe has to deal with, particular attention has to be paid to the thruster that the satellite should rely on. Because of the low mass constraint that needs to be set to keep the costs of the mission low, depending on an enormous amount of chemical propellent to accelerate the spacecraft is something that has to be avoided [2]. For these reasons, significant attention has been directed towards the concept of propellant-free satellites, in particular focusing on the use of solar sails which will be deepened in this work. Indeed, multiple kinds of lightsails exist, and a precise analysis to decide the technology to hinge the entire mission will be carried out.

In addition to the propulsion system, another fundamental part of the mission that must be studied, is the nature of the spacecraft payload. As mentioned before, to keep the costs of the job bounded, a particular attention on the mass of the probes has to be kept. The design specifications for the payload described in [3], suggest a mass limit of around 1 kg. This restriction heavily affects the configuration of the probe, limiting to the essential the systems and instrumentations that will be allowed to be carried on the spacecraft. Moreover, in order to comply with the economic restrictions set at the beginning of the study, the development of completely new technology should be avoided, which is why the exploitation of existing tools will be preferred. Regarding the payload, it has been suggested to lean on the CubeSat architecture, a design standard for nanosatellites based on units of 10 cm cubical probes with a mass of up to 1.33 kg [4].

Among all the systems that will be part of the probe's payload, one has to be treated with particular attention: the communication system. Indeed, even if the spacecraft were operating successfully and gathering valuable data, if these information could not be transmitted, the entire mission would be rendered pointless.
Two main aspects of the communication system will be deepened in this work: the technology that the system will leverage and the technical parameters that have to be tuned to ensure a reliable and effective exchange of data.
As regards the technology used, the apparatus relies on an optical communication system which is derived from the already existing technologies used in the LCRD and LLCD missions [5–7]. The choice of using optical communication instead of the usual radio frequencies is based on the fact that with laser communication it is possible to achieve much higher data rates than the once reachable with RF and that the optical spectrum is not regulated as the RF is [8, 9].
Regarding the technicalities of the communication, various calculations will be presented to properly set the structure of the mission. Because of the limited mass and power available to each probe, it immediately appears clear that a single spacecraft will never have the chance to be able to transfer the gathered data from the foreseen distances to the Earth. As a consequence of these limitations, [3] proposes to build a swarm of nanosatellites (see Figure1.1) that will be used to hop the information from the furthest probe to a receiver located on the Earth's surface. This approach is the cornerstone of this work, and all the subsequent reasonings and strategies presented are tailored to leverage this topology.

Considering these settings, a new fundamental question has to be addressed: how much should

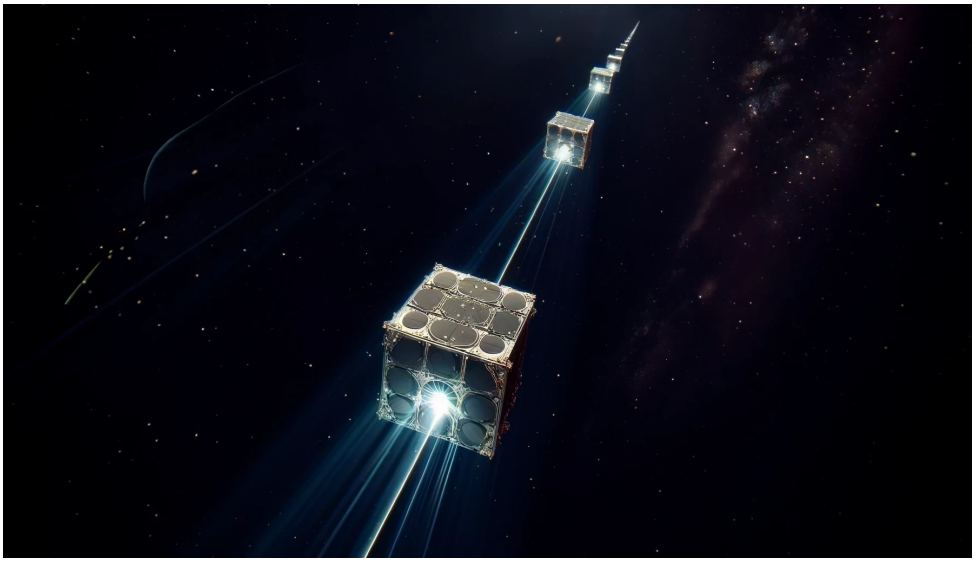

Figure 1.1: Representation of the swarm [1]

the probes be far apart so that they would be able to efficiently communicate with each other? The solution to this underlying problem is presented in multiple ways in this thesis. Indeed, the parameters that directly affect the results are several (transmitting power, modulation scheme, receiving apparatus, etc..), and for each of these, a possible result is proposed.

Finally, to ensure the system's reliability, multiple margins and redundancies are implemented, providing numerous opportunities to continue this research and advance with future studies.

The successive chapters are organized as follows. Chapter 2 will present the architecture of the nanosatellite deepening the design of the lightsails and the embedded systems of the payload. In Chapter 3 the communication apparatus of the probes is analysed. This section outlines the rationale for choosing the optical spectrum over RF frequencies and describes the equipment, derived from the LCRD and LLCD missions, that will be utilized in the discussed context. Chapter 4 examines the technical details of the transmission apparatus, providing some comprehensive calculations regarding the distances between each probe once the expected behaviour of the swarm is set. After providing such computations, based on the results of the analysis, the previously mentioned redundancies techniques are exposed. In conclusion, in Chapter 5 and 6 are respectively reported some proposals to be investigated in future works and the conclusions that can be drawn from this thesis.

[1]Note that the image has been generated via an AI tool. Moreover, the picture does not intend to give a precise representation of the architecture of the nanosatellites or of the communication systems, but rather to give the reader an approximate intuition of the topology of the swarm and of the settings of the thesis.

Chapter 2

The nanosatellite architecture

The architecture of the space probe can be simply broken down into two main components: the light-sail (Section 2.1) and the payload (Section 2.2).
Since one of the main purposes of the entire project is to develop a cheap, scalable and efficient means to explore the Solar System and beyond, one of the main constraints of the project is the mass budget [3].
Mass is a crucial factor when dealing with extraterrestrial activities. The first technical and economic challenge is faced when the probe has to leave the Earth. Since this is usually done via a rocket launch, the related costs are directly proportional to the mass of the rocket payload, making pivotal the minimization of useless weight-budget consumption [10].

Despite missile launches are still the main means to move objects and people to orbit, cheaper solutions which can lead to up to 90% savings [12] are being developed. SpinLounch [13], a private company founded in 2015, is developing a system which accelerates small payloads in a circular movement, and uses the kinetic energy gathered, to shoot lightweight orbiters into space. As mentioned earlier, the extreme cost reductions and the opportunity to launch multiple probes per day [12], make this new technology a remarkable innovation for these purposes.

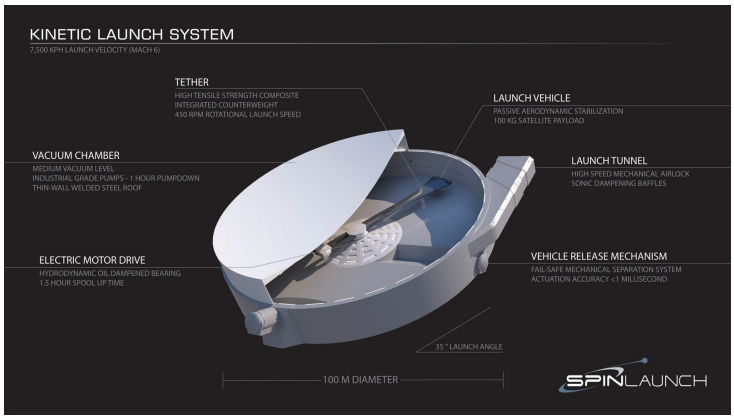

Figure 2.1: SpinLaunch system diagram [11]

Another important reason that leads to mass constraint is the propulsion system. Since the chosen thrust mechanism is a lightsail, a critical restriction has to be set on the mass of the payload. Even if Lightsails allows to reach relativistic speeds [14], this can only be achieved with low-mass payloads [15].

2.1 The lightsail

2.1.1 Chemical propulsion

From Newton's first law, the only available method to generate thrust in vacuum, is to eject some mass with a certain velocity out of the spacecraft to generate momentum. According to [3], the equation

$$F = \dot{m} V_{ex}$$

where $\dot{m}$ is the *mass consumption rate* [kg/s] and V_{ex} is the exhaust velocity of the expelled mass, with a *chemical propulsion* system [16, Chemical propulsion], it is possible to generate a force equal to the product of $\dot{m}$ and V_{ex}. Even if this method is extremely powerful and features a high *thrust-to-mass* ratio, exploiting such technology would be impossible for our purposes due to the unacceptable propellent mass [17].

2.1.2 Photonic thrusters

Because of the mass constraint, and the need to generate some momentum to accelerate the spacecraft, lightsails represents the best choice for this work.
A lightsail, also known as a *solar sail* or *photon sail*, is a method of spacecraft propulsion using radiation pressure reflected by a large mirror.
Even if photons do not have a mass, they do have an energy $U = hf$, and therefore a linear momentum [18]

$$p = \frac{U}{c} = \frac{hf}{c} = \frac{h}{\lambda} \tag{2.1}$$

where:

p is the momentum,	U is the energy,	f is the frequency,
λ is the wavelength,	c is the speed of light,	h is Planck's constant.

This linear momentum can be used by the lightsail in order to accelerate a light payload.
Because of mass constraints, lightsail are often built via a thin layer of reflective materials which

can be made out of TiO_2 or *Kapton* [3], with a thickness in the orders of the nm [14].
In the scenario analysed in [3], the lightsail is supposed to drive a 1 kg payload with a surface, in a worst-case scenario, of 10 m^2.
The sail is sustained by a structure made of four carbon-fibre booms arranged in a four-petals shape. Depending on the design of the lightsail, whether it is a square (Figure 2.2) or circular, the mass budget that has to be allocated to the sail is respectively 276 g or 249 g.

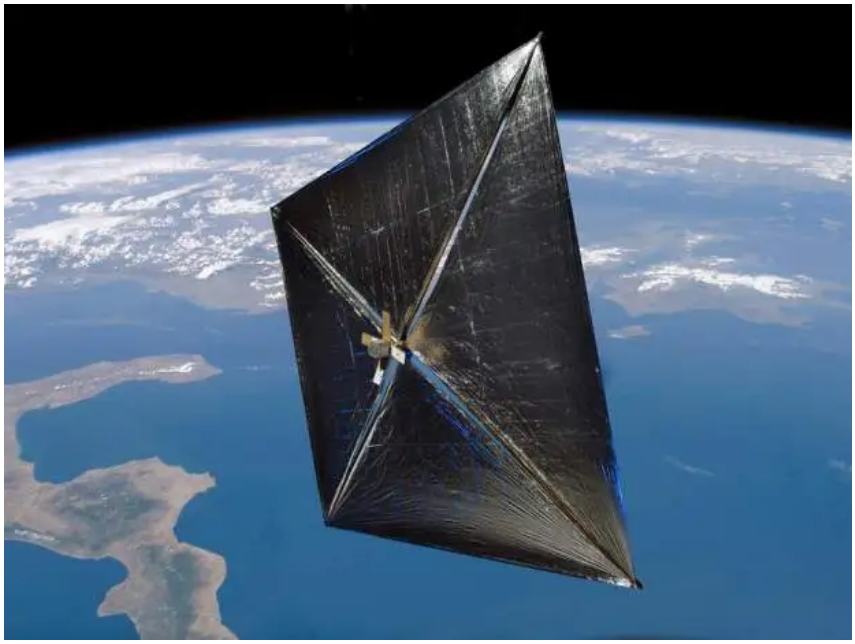

Figure 2.2: Lightsail [16, Solar sail demonstrator]

Given these conditions, and the formula proposed in [14] and revised in [3]:

$$P = \frac{I_0}{c}(A + 2R) \tag{2.2}$$

with an ideal lightsail (R = 1, A = 0) and a laser irradiance of $I_0 = 10$ GW/m, the pressure on the surface will be of $P \simeq 70$ Pa, which in a sail of 10 m^2 is equivalent to a force of [19] :

$$F = PA = 70 \cdot 10 = 700 \text{ N}$$

capable of accelerating a 1 kg payload up to 700 m/s^2 and allowing it to reach 20% of c in around one day (23.8 h) of exposure. [1]

[1] Clearly this numerical solution has to be taken as a reference instead of a real solution. Indeed it is not possible to expose the lightsail uniformally for 24 hours. This has to do with the fact that a base station on Earth should be responsible for generating the laser beam, and due to the rotation of the planet, there will be periods (half of each Earth rotation) by which there is no LOS between the lightsail and the laser-generating-system. Moreover, it is

Propellent-less photonic thruster

The thrust mechanism just describe is part of the *propellent-less* [17] photonic thrusters group [20]. These can be further divided into two groups:

1. **Systems with external light sources**: the radiation emitter is external to the spacecraft. The example previously analysed is part of this group since the generator of the laser beam has been chosen to be on Earth's surface.

2. **Systems with onboard light sources**: in this case, the emitter is part of the spacecraft. Because of the limited power budget usually set on probes, a clever mechanism to enhance the performance of this implementation is to reflect the laser beams multiple times between two opposite mirrors. Assuming a high reflectance of these, we could multiply the effects of photons' momentum to increase the acceleration of the spacecraft.

Propellent-based photonic thrusters

Another acceleration mechanism based on radiation is the so-called *propellent-based photonic thrusters* [17]. In this scenario the energy of the laser beam reaching the probe causes ablation [21] on the lightsail, generating an acceleration. In the scenario analysed in this thesis and in [3], this thruster is not studied, but future works could consider such type of application.

2.1.3 Manouver

As explained at the beginning of (Section 2.1.1) the easiest way to accelerate, and therefore manoeuvre, a spacecraft in vacuum is to expel material. However, because of mass constraint, in our scenario this technique has to be replaced by a manoeuvring mechanism that takes advantage of the lightsail propulsion system.
As explained in [1], trajectory setting and spacious manoeuvering is accomplishable via suitably orienting the lightsail in order to change the direction of the force applied to the sail itself. In [1], the lightsail is considered to be only driven by solar radiation, therefore the three main manoeuvering mechanisms are the following:

1. Align the sail perpendicular to the Sun radiation to reach maximum acceleration

2. Align the sail parallel to the Sun radiation in order to minimise the acceleration

important to note that expecting a constant irradiance while the probe is moving is not realistic, this will therefore further diminish the pressure that the lightsail will experience while accelerating. Computing and analysing in detail the lightsail behaviour goes beyond the focus of this thesis and could be the object of other works, for example [1, 14, 15, 17]

3. Set the solar sail with a suitable angle w.r.t. the Sun, so that the force vector is set to be opposite to the motion of the spacecraft.

Clearly, some of the possibilities shown in [1] are not practical to the purpose of the mission that is being studied. First of all, the sail considered is not supposed to be driven by Sun's radiation, but rather from a laser emitting source. Because of the relative position of the probe and the beam emitter, it would be impossible to generate a force which has no component with the same direction of the spacecraft motion. Moreover, it would also be useless to rotate the sail so that the radiation of the laser is parallel to the surface of the lightsail. Again, since the radiation source is a laser, it will be much easier and energy-conservative to simply switch off the laser. Certainly, what can be taken by the previously described system, is the possibility to rotate the sail w.r.t. the incoming beam. This could lead the probe to change the direction of its vector velocity $\vec{v}$ to fix a desired trajectory. Even if solarsails are not being deepened in this thesis, it would be interesting to go into details of solarsails to make the proposed scenario more energy efficient.

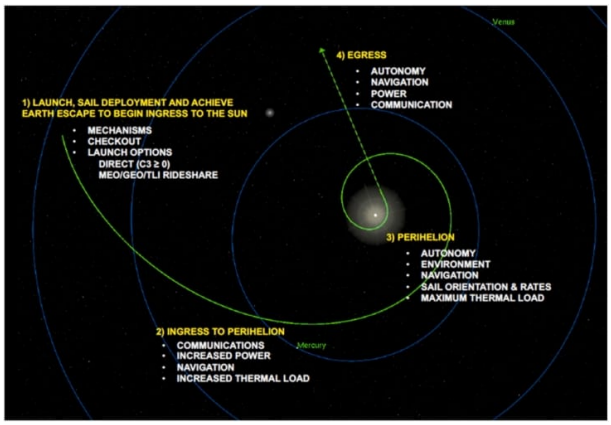

Figure 2.3: Trajectory of solarsail [1]

As described in [1], we could use solar energy to accelerate the probe towards outer space. Instead of pushing the spacecraft out of the Earth's orbit immediately directed to the limit of the Solar System, we could set a trajectory which will lead the spacecraft to firstly approach the Sun (see Figure 2.3) and then exploit the high intensity of the solar radiation to accelerate in the direction of the edge of the Solar System. This choice is not only energy efficient, but it also allows the probe to gather data (for example of Space Weather [1]) between the Earth and the regions close to the Sun.
Clearly, more adjustments should be made, the probe should be specifically designed to work in near-sun environment [22] which is not a trivial task.

2.2 The payload

The term payload was originally referring to the goods and products that cargo ships were transporting through the sea. In the space mission field, when we talk about "payload", we refer to the instruments and the equipments that are carried by the spacecraft [23, 16, Payload systems]. As mentioned before, because of the chosen propulsion system, the mass available for the pay-

load is extremely limited. As described in [3], the payload foreseen for such a mission is estimated to weigh around 1 kg. Also, in order to reduce costs, it is preferred to rely on COTS devices which can be tested and adapted to work in space.
Because of these constraints, a suitable option for the payload design is the CubeSat standard [3, 15, 24].

2.2.1 CubeSat

Originally conceptualized as educational tools or low-cost technology demonstration platforms, CubeSats were envisioned to be developed and launched within a short timeframe of one or two years. However, in recent times, there has been a notable evolution in CubeSat missions. Advanced CubeSat projects have emerged [25], signifying a transition from their initial educational and technology demonstration roles. Instead, they now offer opportunities for conducting low-cost, real science missions with the potential for significant scientific advancements and generating commercial revenue. This shift underscores the expanding versatility and potential impact of CubeSats in space exploration and research endeavours [4]. The CubeSat standard mandates that the probe dimensions be confined to a cube measuring 100 mm per side, with a maximum mass of 1 kg. These specifications render the CubeSat platform an ideal selection for the mission's objectives [26].

2.2.2 Embedded systems

Even if specifying the scope of the mission and the devices expected to be part of the probe payload is not within this thesis domain, some details regarding the minimum onboard equipment required to accomplish the mission can be given[3].

Reaction wheel

One of the most important components which perfectly suits the mass and power budget, and accomplishes its fundamental role, is the reaction wheels. A reaction wheel is a device used in spacecraft to adjust and maintain their attitude in space. It works by spinning a wheel in one direction, causing the spacecraft to rotate in the opposite direction because of angular momentum conservation [19]. By controlling the speed and direction of rotation of the reaction wheel, the spacecraft can be manoeuvred and stabilized without using propellant, which is one of the key constraints of the project [27, 28].

Power generation system

Generating power and storing energy is crucial for deep space exploration. As usually done [16, What powers a spacecraft] in space, power is generated via solar panels and stored via lithium batteries [29]. As shown in [3] the mass budget allocated for both the solar panels and the Li-Ion battery is of 100 g each.

The study by [3] calculates that the solar array can generate an average power of approximately 3000 mW. However, this value should be regarded as a reference, as it is based on an assumption of the probe being at a distance of around 1.5 AU from the Sun, similar to the distance between Mars and the Sun. Since the spacecraft is expected to travel well beyond Mars, a more comprehensive power-budget analysis should consider the decrease in solar irradiance as the spacecraft moves farther from the Sun. This decrease in irradiance raises the possibility of insufficient power generation, necessitating careful planning and consideration in the spacecraft power management strategy.

A possible solution to this issue, could be represented by the use of a laser beam not only to accelerate the probe, but also to power the systems in the spacecraft [30]. Part of the energy carried by the beam could be transferred to the solar panels solving the problem of power lack, while moving away from the solar system (Figure 2.4).

Figure 2.4: A laser from the Earth to power the solar array [30]

When considering solar panel configurations for space probes, multiple options exist. However, in the context of nano-satellites [29], two scenarios emerge as the most realistic. The first scenario follows a classical approach, wherein the probe deploys solar cells by unfolding the photovoltaic system and initiating solar energy collection [31, 32]. Alternatively, the second option involves utilizing a ”smart skin” [30], which envelops the CubeSat exterior surface. While this latter solution may yield lower energy production efficiency, it significantly reduces

the risk of mechanical failures due to the absence of moving parts required for the deployment.

Instrumentation

Even if it has been said that the scope of this thesis is not to explicitly define a purpose for the mission, following [3] we present a possible measuring system which could be of interest for a project like the one described. The instrument considered is a planar Langmuir ion probe [33, 34], which is a specific kind of sensor capable of analysing temperature, density and potential of plasma. This kind of instrumentation is typically used to map the heliosphere plasma and to analyse the planets close environment [15].
What is of particular interest to us is the mass and power budget. The sensor is foreseen to weigh around 50 g and the peak absorption power is estimated to reach 250 mW.

Communication system

The spacecraft communication system will exclusively utilize light-based communication. Recognizing its central importance, a dedicated chapter in this thesis is allocated to thoroughly discuss this primary topic.

Subsystem	Technology	Weight [g]	Power [mW]
Sensor	PLP	50	250
Communications	Transmitter	100	2000
	Receiver	100	
ADCS	Sun sensor (coarse)	40	100
	Sun sensor (fine)	5	40
	Reaction wheels (3)	150	300
	Desaturation thrusters	240	30
C &DH	Core PCB	5	–
	CPU	1	5
T/S	Alloy support	100	
	Filler/harness	20	
	Blanket	60	
Power	Solar array	100	(- 3000)*
	Battery	100	
	PPU	20	50
Total estimate		1097	2920

Figure 2.5: Estimated mass and power budget [3]

Chapter 3

Communication System

One of the primary systems, if not the most critical, aboard the spacecraft is the communication apparatus. Its significance cannot be overstated, as the success of any scientific exploration hinges on the ability to receive and transmit data. Without this capability, the entire endeavour would be rendered ineffective and futile.
As remarked earlier, because of the design constraints of the mission, the mass and power budget available to this crucial system is extremely limited [10]. [3], which is our reference for the design of the probe and the lightsail, assumes that the average power available to this module is expected to be around 2000 mW and that the mass budget granted is of 100 g for both the transmitter and the receiver.

3.1 Radio frequency

One of the most common carrier frequency used nowadays in telecommunications is the radio frequencies [8]. RF communications encompass a broad range of electromagnetic frequencies commonly used for wireless communication, including radio waves, microwaves, and other longer wavelength signals. RF communication is widely used in various applications, such as radio broadcasting, cellular networks, Wi-Fi, and Bluetooth [9].
Radio frequencies have also been widely used in space communications systems, the DSN

Figure 3.1: Deep Space Network antenna [16, What is the deep space network?]

(Deep Space Network) is an array [8] of antennas, suitably arranged in different locations on the Earth's surface responsible for most of the telecommunications between Earth and spacecrafts [35].
Even if radio frequencies are well known and widely used, two fundamental critical issues have to be taken into account: the limitations and regulations to which RFs are subject to [8, 9], and the low bandwidth available, which can lead to limited datarates capabilities.

3.2 Optical communication

Optical communication offers several advantages over radio frequency for deep-space communication. Firstly, optical frequencies are not subject to the same regulatory restrictions as RF frequencies [36], allowing for more flexibility and potentially higher data transmission rates. This means that optical communication systems can utilize higher bandwidths, enabling faster data transfers compared to RF systems [8, 9].
Because of these reasons, for the mission being considered in this thesis, an optical communication system will be used, exploiting the advantages mentioned before.

This work will draw upon existing optical communication technologies as the cornerstone for constructing the communication system for the mission described until now. By harnessing established optical communication solutions, our goal is to streamline mission costs and circumvent the necessity of creating new telecommunications technology from scratch.

3.2.1 Lunar Laser Communication Demonstration (LLCD)

Also known as LLCD (Figure 3.3) [7], the Lunar laser Communication Demonstration has been one of the first approaches to laser communication in space environment.
In the spring of 2008, NASA initiated a program to deploy a new compact spacecraft into lunar orbit. This science mission aimed to gather data on the composition of the lunar atmosphere and study the lunar exospheric dust environment. Shortly thereafter, it was realized that this spacecraft had additional capacity to accommodate one more small payload, presenting an opportunity to conduct

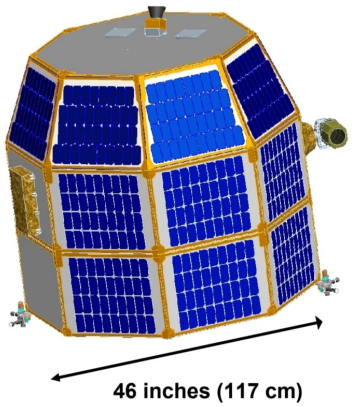

Figure 3.2: Lunar Atmosphere and Dust Environment Explorer [7]

a technology demonstration of laser communication [37]. Thus, the Lunar Laser Communications Demonstration (LLCD) project was established.

The primary science mission, known as the Lunar Atmosphere and Dust Environment Explorer (LADEE) [37], was managed by the NASA Ames Research Center (ARC). The spacecraft, developed by ARC, is based on their modular bus design, as depicted in Figure 3.2. Scheduled for launch aboard a Minotaur V rocket from Wallops Island, VA in mid-2012, this versatile craft was expected to be the first of many cost-effective missions to explore the Moon and potentially beyond.

The key objective of LLCD is to showcase the feasibility of achieving high-speed laser communication from a compact terminal at lunar distances. LLCD comprises three main components: the Lunar Lasercom Space Terminal (LLST), the Lunar Lasercom Ground Terminal (LLGT), and the Lunar Lasercom Operations Center (LLOC). The primary objective

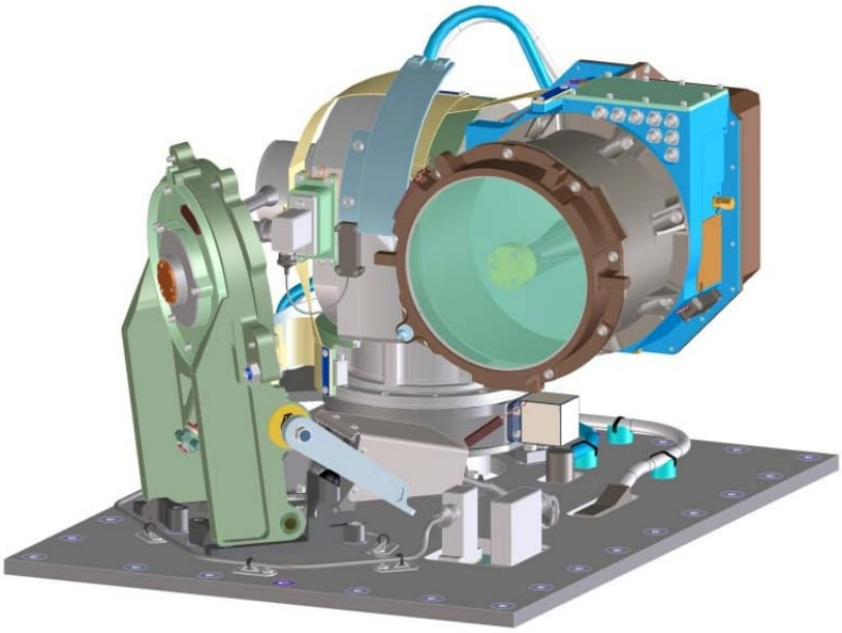

Figure 3.3: The Lunar Laser Communication Demonstration (LLCD) [5]

of LLCD is to prove the practicality of optical communication with a probe in an extraterrestrial environment, by achieving data transmission rates of up to 622 Mbps on the optical downlink and up to 20 Mbps on the optical uplink. To accomplish this, the Lunar Lasercom Space Terminal (LLST), illustrated in Figure 3.4, is composed of three modules: an Optical Module, a Modem Module, and a Controller Electronics Module. The fully gimballed Optical Module is positioned on an external surface of the small spacecraft, while the other two modules are housed internally. Connections between modules are established via electrical and optical fiber

harnesses. The LLST operates across three wavelengths spanning from 1550 nm to 1570 nm. The Optical Module features a 2-axis gimbal, leveraging COTS components, a 10-centimeter reflector telescope, a spatial acquisition detector, and fiber-coupling optics. The acquisition detector, functioning as both a receiver and a tracking sensor, is a simple quadrant detector [6, 7, 38, 39].

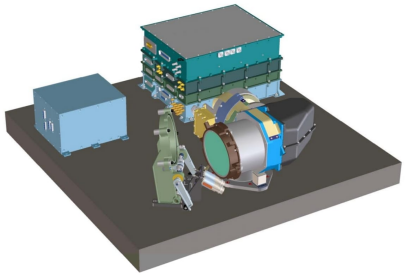

Figure 3.4: Lunar Lasercom Space Terminal [7]

The successes gained by this mission proved finally that the technology for laser communication was mature enough to be implemented as the primary communication method in space telecommunications. Thanks to its high bandwidth and limited power requirements, optical communications have quickly been exploited for further projects which lead to the development of the Laser Communication Relay Demonstration (LCRD).

3.2.2 Laser Communication Relay Demonstration (LCRD)

The Laser Communications Relay Demonstration Project (LCRD) (Figure 3.5) is a collaborative effort involving NASA's Goddard Space Flight Center (GSFC), the Jet Propulsion Laboratory at the California Institute of Technology (JPL) and the Massachusetts Institute of Technology Lincoln Laboratory (MIT/LL). LCRD aims to deliver two years of uninterrupted high data rate optical communications in an operational setting [41]. This demonstration showcases how optical communications can address NASA's growing demand for higher data rates, or alternatively, how it enables the use of lower power and lower mass communication systems on user spacecraft, w.r.t. comparable RF systems. Moreover, LCRD architecture allows it to serve as a space-based testbed for the development of additional symbol coding, link, and network layer protocols [5].

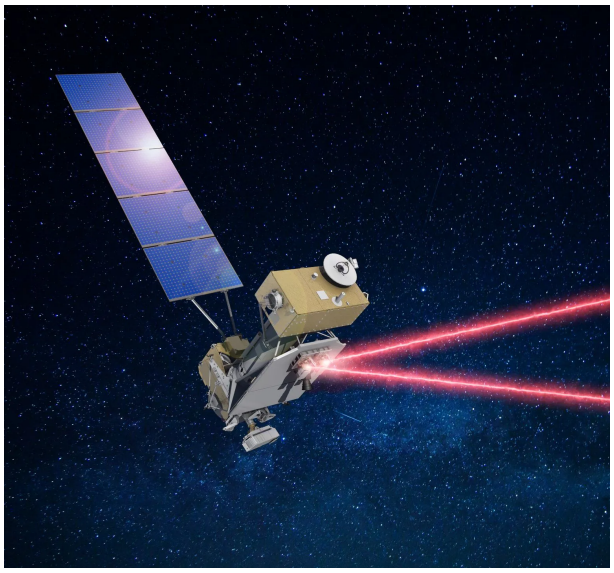

Figure 3.5: Laser Communication Relay Demonstration [40]

As stated in the name, the LCRD is supposed to work as a relay, a component that receives data from one network segment and forwards it to another. Relays are often used to extend the range of a network by forwarding data between segments that are physically separated or to connect different types of networks [42]. In the context of the Laser Com-

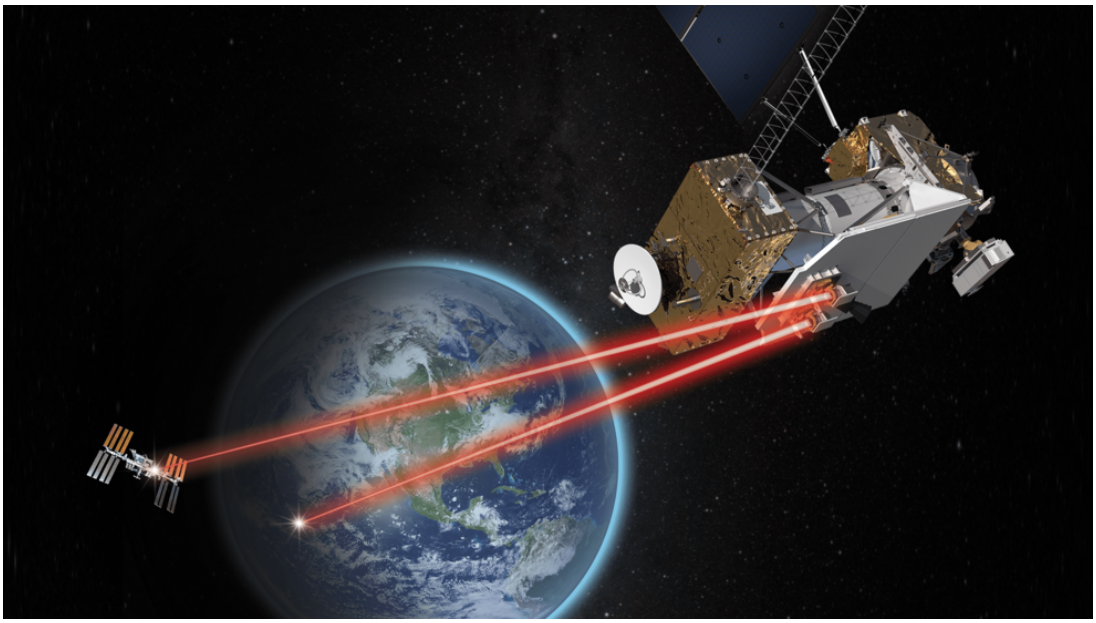

Figure 3.6: ILLUMA-T [16, First Two-way End-to-End Laser Communications Relay System]

munications Relay Demonstration (LCRD), the term ”relay” refers to the satellite equipped with laser communication terminals that receive data from user spacecraft or ground stations and relays it to its destination, such as another spacecraft or a ground station. LCRD serves as a communication relay in space, facilitating the transmission of high-speed optical data between different points in Earth's orbit or between space and ground-based stations [40]. In addition, LCRD will exemplify its capabilities by relaying data between the International Space Station (ISS) and Earth via the ILLUMA-T (Figure 3.6) system, showcasing its versatility and potential for facilitating efficient communication links for space missions. This demonstration serves as an example of how LCRD can be utilized to enable seamless data transmission between space-based assets and ground-based stations, supporting various scientific research and operational activities in space [16, ILLUMA-T].

Ground terminals

The LCRD Ground Segment consists of the LCRD Mission Operations Center (LMOC) and two ground stations. The LMOC is responsible for all scheduling, command, and control operations related to the LCRD payload and the ground stations [41].

Figure 3.7: OGS-1 [5]

Each Earth ground station serves three primary functions when communicating with one of the two optical communications terminals on the GEO spacecraft: receiving the communications signal from the GEO space terminal, transmitting a signal to the GEO space terminal, and emitting an uplink beacon beam to ensure the GEO space terminal is accurately aligned with the Earth's location. The receiver on Earth must possess a collector of sufficient size to capture ample power to support the data rate, efficiently couple this light onto low-noise detectors while minimizing background light interference, and execute synchronization, demodulation, and decoding of the received waveform.

Regarding the uplink beacon, each Earth ground station transmits a reference signal to establish the beam-pointing direction of the GEO space terminal. Turbulence effects are a significant factor in determining the laser power required for a ground-based beacon since they cause beam dispersion, reducing mean irradiance at the space terminal and leading to fluctuations in the received power [5]. The two ground stations, which are referenced as OGS-1 (Figure 3.7) and OGS-2, have been located on Table Mountain in Southern California, and in Haleakalā, Hawaii – a volcano in Maui. The choice of these two locations has to be traced back to the need for good weather conditions in order to achieve effective communication while dealing with optical links [8] [16, Lcrd-ground segment].

Modems and modulations

A fundamental part of the design of a communication system is the choice of the correct modulation. In the context of LCRD two main modulations have been chosen: Photo counting Pulse Position Modulation (PPM) and Differential Phase Shift Keing (DPSK).

PPM Photon counting PPM is notably efficient in terms of photon usage (and therefore power), though detector capabilities and the need for quicker electronics constrain its maximum data rate. The LCRD project utilizes the cost-effective PPM modem originally developed for NASA's LLCD (Section 3.2.1) to generate a PPM signal. This modem accommodates a downlink that varies from 39 to 622 Mb/s and an uplink ranging from 10 to 20 Mbps, exploiting respectively 16-PPM and 4-PPM [5]. Because of high power efficiency and low capabilities of

facing fading and noise, PPM is preferred to DPSK when dealing with deep-space telecommunications.

DPSK LCRD will also incorporate Differential Phase Shift Keying (DPSK), which is noted for its excellent noise tolerance, fading endurance, ability to handle extremely high data rates, and capability to maintain communications even when the Sun is in the field of view. Utilizing a DPSK modem previously developed by MIT/LL, LCRD adopts a cost-effective method for generating DPSK signals. This modem is capable of transmitting and receiving data at rates ranging from 72 Mbps to 2.88 Gbps (uncoded), with the possibility to further enhance the modem to support speeds exceeding 10 Gbps. The DPSK modem uses the same signalling method for both uplink and downlink, encoding data by the phase differences between consecutive pulses [8, 9, 43].
Because of the high tolerance to noise and fading, DPSK is often preferred to PPM for space-Earth communication. In contrast, the choice for deep-space communication is often left to PPM since the second is more power efficient than the first one [5].

Chapter 4

Link Budget

In telecommunications, the link budget is an accounting of all the gains and losses from the transmitter, through the medium (e.g.: copper cable, fibre optic, free space) to the receiving communication system [9]. This is often used to properly set different variables of the communication system such as the transmitting power, the modulation scheme, the distance between the transmitter and the receiver and so on [43].

The main purpose of this thesis is indeed to analyse the possibly tunable variables and the constraints of the systems to develop a reasonable scenario to make the apparatus working properly.

4.1 The scenario

The scenario to which we reference is the one described in [3], by which a swarm of nanosatellites, driven by solar sails, are used to explore the boundaries of the solar system and beyond.
The basic scheme that we analyze is a train of aligned nanosatellites which creates a linear topology of hops, through which the information will travel (Figure 4.1).
In detail, because of the low power budget available to the nanosatellites [3], the communication system will never be able to send information to the Earth. Therefore, the solution adopted to overcome this issue is that each probe will receive the data from the preceding one and will forward it to the following nanosatellite. In this way, no information will hopefully be lost and the power constraint will be fulfilled [8].
In this scenario, the basic variable that has to be tuned is the distance between each probe [43]. This value needs to be not too big, in order to not come across information loss, and not too small, otherwise we will have to send too many space probes and the costs of the mission will increase dramatically [9].

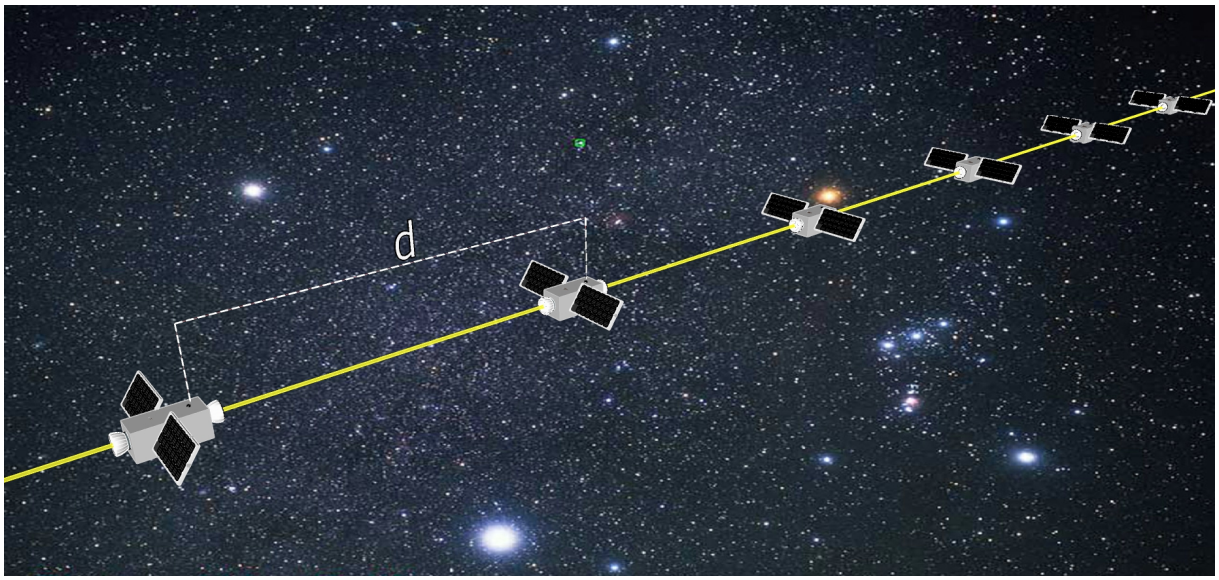

Figure 4.1: Scenario

Another tunable variable that is available, is the choice of the modulation scheme adopted. Since the mission should be cost-conservative, in this work we prefer to rely on existing technologies. Because of this, the communication system that has been chosen will be the one adopted for the LCRD (Section 3.2.2) and the LLCD (Section 3.2.1), so the modulations that will be analyzed are both PPM and DPSK.

4.2 The computations

In order to obtain some values of the distances that the probes can be apart, we first need to choose the modulation scheme that we want to reference to, and the Bit Error Rate BER (or bit error probability P_b) acceptable. Once this has been done, based on the available formulas, a value d for the distance between each probe can be computed.

In this thesis several values of d will be computed based on the different modulation schemes adopted, in particular we will focus on:

1. 16-PPM
2. 8-PPM
3. 4-PPM
4. 2-PPM
5. 16-DPSK
6. 8-DPSK
7. 4-DPSK
8. 2-DPSK

The BER chosen will be 10^{-9}, this is just a conventional value and all the calculations performed from now on could be done again by choosing a different BER value [8].
Also, it is important to note that, because of the choice of limiting costs by using existing tech-

nologies, all the values of the variables related to technical information of the communication system, are related to the optical communication apparatus used in LCRD and LLCD missions.

Ultimately, to perform the computations of the link budget, from now on we will reference the formula reported below, which has been taken from [43]:

$$SNR = \frac{P_{Tx}}{k\ T_{eff,Rc}\ B\ a_{Ch}} \tag{4.1}$$

where:

SNR is the Signal to Noise Ratio,	P_{T_x} is the Transmitted power,
k is the Boltzmann constant,	$T_{eff,Rc}$ is the effective noise temperature at the receiver,
B is the bandwidth,	a_{Ch} is attenuation of the channel.

4.2.1 Technical parameters

To properly use the formula above, some values that are strictly related to the technicalities of the communication system need to be found. The complete list of these values is provided here below:

Transmitted power P_{Tx}

The value of P_{Tx} is 2W which is taken from [3].

Effective noise temperature at the receiver $T_{eff,Rc}$

The formula for the effective noise temperature has been taken from [43] which is:

$$T_{eff,Rc} = T_0\ [F - 1] \tag{4.2}$$

The value for T_0 is set to 290 K as stated in [43] and the value for F is taken from [39], which references [44], which provides a value of 3 dB for the noise figure. Therefore, the effective noise temperature at the receiver is computed to be:

$$T_{eff,Rc} = T_0\ [F - 1] = 290\ [10^{\frac{3}{10}} - 1] = 288.63\ \text{K}$$

Channel attenuation a_{Ch}

The attenuation, from [43], is just the inverse of the path loss $a_{Ch} = L_{Ch}^{-1}$. Then, the formula for the path loss is taken from [43] and [8], by which:

$$L_{Ch} = D_t \; D_r \; \left(\frac{\lambda}{4 \; \pi \; d}\right)^2 \tag{4.3}$$

where D_t and D_r are respectively the directivity of the transmitter and the receiver.
As per [6], λ is set to 1528.17 nm.
From [8] and [45], the expression for the directivity D is:

$$D = \frac{4\pi}{\Omega_A} \tag{4.4}$$

where Ω_A is the solid angle of the beam. To compute the solid angle Ω_A of the beam we rely on [18] and [46], so:

$$\Omega_A = 2\pi(1 - \cos\theta), \tag{4.5}$$

where θ is the beam angle. The value of θ is taken from [39] and [5], which provide $\theta = 15$ μrad. Therefore:

$$\Omega_A = 2\pi(1 - \cos(15 \cdot 10^{-6})) = 706.859 \cdot 10^{-12} \text{ sr}$$

and so

$$D = \frac{4\pi}{706.859 \cdot 10^{-12}} = 1.78 \cdot 10^{10}$$

In conclusion, from 4.3, 4.4 and 4.5 the channel loss is:

$$L_{Ch} = D_t \; D_r \; \left(\frac{\lambda}{4\pi d}\right)^2 = \left(1.78 \cdot 10^{10}\right)^2 \; \left(\frac{1528.17 \cdot 10^{-9}}{4\pi}\right)^2 \; d^{-2} = 4.69 \cdot 10^6 \; d^{-2}$$

Bit Error Rate

The equation for the BER depends on the modulation scheme [43]. Because the following work will be based on two modulation schemes: PPM and DPSK, both BER formulas are provided. The expression of the BER for the PPM modulation scheme is provided in [47]:

$$P_b = BER_{PPM} = Q\left(\frac{1}{L-1}\sqrt{\frac{L\log_2(L)}{2}}\sqrt{SNR}\right) \tag{4.6}$$

where L is the number of symbols of the PPM modulation.
Morover, the expression for the BER related to DPSK modulation is found in [43]:

$$P_b = BER_{M-DPSK} = \frac{2}{\log_2 M} Q\left(\sqrt{2\ SNR}\ \sin\left(\frac{\pi}{M}\right)\right) \quad for \quad M \geq 4 \tag{4.7}$$

and for $M = 2$ the BER expression becomes:

$$P_b = BER_{2-DPSK} = Q\left(\sqrt{2\ SNR}\right) \quad for \quad M = 2 \tag{4.8}$$

Bandwidth B

To compute the bandwidth B associated with PPM, the data rate is set to 1 Gbit/s for a modulation scheme using L-PPM, where L = 16.
With these settings, $\frac{10^9}{\log_2 L}$ words/s are transmitted, leading to a word time T_w of $\frac{\log_2 L}{10^9} = 4$ ns (T_w: the time required to send a word).
Extending this reasoning to the general case, given $T_w = 4$ ns, it follows that:

$$T_{\text{bit}} = \frac{T_w}{\log_2 L} = \frac{4 \cdot 10^9}{\log_2 L} \tag{4.9}$$

therefore, from [48], the minimum bandwidth B_{0-PPM} is calculated as:

$$B_{0-PPM} = 2 \cdot \frac{1}{2\,T_{\text{bit}}} = \frac{\log_2 L}{T_w} \tag{4.10}$$

Assuming the pulse shape used for PPM is a raised cosine with roll-off factor $\beta = 0.8$ [8, 9, 43, 49] to simplify sampling synchronization, and given that bandwidth requirements are less stringent due to the unregulated spectrum in optical communications, then, by [9] and [43], the actual bandwidth B utilized is:

$$B_{PPM} = B_{0-PPM}(1+\beta) = \frac{\log_2 L}{T_w}(1+\beta) \tag{4.11}$$

The above reasoning has been developed for PPM modulation, the formulas reported below are instead focused on computing the bandwidth B for DPSK modulation.
Assuming $T_w = 4$ ns to ensure the same time synchronization as before, from [43] it is found that $B_{0-DPSK} = \frac{1}{T}$ where $T = \frac{T_w}{2}$. Therefore:

$$B_{0-DPSK} = \frac{2}{T_w} \tag{4.12}$$

and

$$B_{DPSK} = B_{0-DPSK}(1+\beta) = \frac{2}{T_w}(1+\beta) \tag{4.13}$$

4.2.2 Distance estimation for PPM

To compute the distance at which the probes have to be set apart, firstly is necessary to invert the BER equation 4.6 expliciting the SNR:

$$\begin{aligned} BER_{PPM} &= Q\left(\frac{1}{L-1}\sqrt{\frac{L\log_2(L)}{2}}\sqrt{SNR}\right) \\ &\Rightarrow \frac{1}{L-1}\sqrt{\frac{L\log_2(L)}{2}}\sqrt{SNR} = Q^{-1}(BER_{PPM}) \\ &\Rightarrow SNR = \left[Q^{-1}(BER_{PPM})(L-1)\right]^2 \frac{2}{L\log_2(L)} \end{aligned} \tag{4.14}$$

where $Q^{-1}(x)$ is the inverse Q function.
Once this has been done, it is possible to substitute in the SNR equation 4.1 the expression for the channel attenuation a_{Ch} found in 4.3 and subsequently explicitate d:

$$\begin{aligned} SNR &= \frac{P_{Tx}}{k\ T_{eff,Rc}\ B\ a_{Ch}} \ \Rightarrow \\ SNR &= \frac{P_{Tx}}{k\ T_{eff,Rc}\ B\ D^{-2}\ \left(\frac{4\pi d}{\lambda}\right)^2} \ \Rightarrow \\ d &= \sqrt{\frac{P_{Tx}\ D^2\ \lambda^2}{k\,T_{eff,Rc}\,B\,(4\pi)^2\,SNR}} \end{aligned} \tag{4.15}$$

To 4.15 we substitute $T_{eff,Rc}$ from 4.2:

$$d = \sqrt{\frac{P_{Tx}\ D^2\ \lambda^2}{k\,T_0\,[F-1]\,B\,(4\pi)^2\,SNR}} \tag{4.16}$$

then we substitute the SNR with the expression found in 4.14:

$$d = \sqrt{\frac{P_{Tx}\ D^2\ \lambda^2\ L\ \log_2 L}{k\ T_0\ [F-1]\ B\ (4\pi)^2\ 2\,[Q^{-1}(BER)(L-1)]^2}}$$

and finally, from 4.11 we substitute the expression for B:

$$d = \sqrt{\frac{P_{Tx}\ D^2\ \lambda^2\ L\ T_w}{k\ T_0\ [F-1]\ (1+\beta)\ (4\pi)^2\ 2\,[Q^{-1}(BER)(L-1)]^2}} \tag{4.17}$$

Now that an expression for d has been found, it is possible to substitute the numerical values found in 4.2.1 and compute the distances for each PPM modulation scheme.
To do the previous computation and estimate the distances for various PPM modulations, we rely on the simple Matlab script reported in Appendix A, which provides the following results:

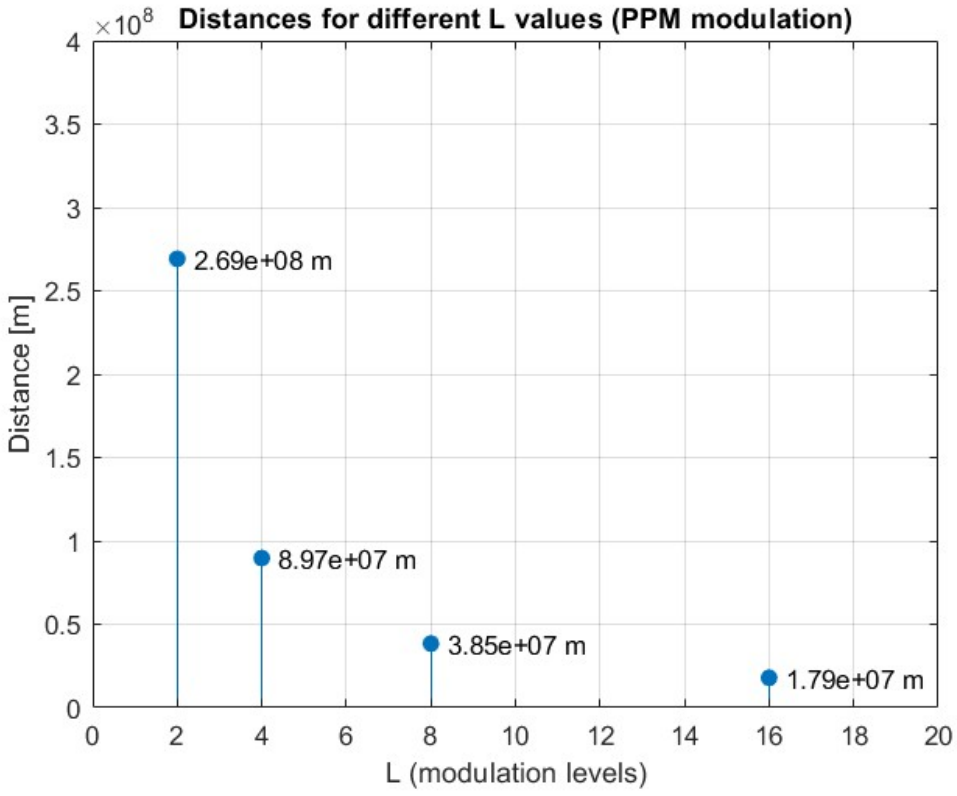

Figure 4.2: Distances related to table 4.1

Table 4.1: Distances for different L values (PPM modulation)

L	Distance [m]	Distance [AU]
2	$2.691727 \cdot 10^8$	$1.799283 \cdot 10^{-3}$
4	$8.972425 \cdot 10^7$	$5.997610 \cdot 10^{-4}$
8	$3.845325 \cdot 10^7$	$2.570404 \cdot 10^{-4}$
16	$1.794485 \cdot 10^7$	$1.199522 \cdot 10^{-4}$

4.2.3 Distance estimation for DPSK

As previously done for PPM modulation, the first thing that has to be done to compute the distances at which the probes have to be set apart when using DPSK, is to invert the equations that relate the BER with the SNR (4.7 ,4.8).
For $M \geq 4$:

$$\begin{aligned} BER_{M-DPSK} &= \frac{2}{\log_2 M} Q\left(\sqrt{2\ SNR}\ \sin\left(\frac{\pi}{M}\right)\right) \\ &\Rightarrow \sqrt{2\ SNR}\ \sin\left(\frac{\pi}{M}\right) = Q^{-1}\left(\frac{BER_{M-DPSK}\ \log_2 M}{2}\right) \\ &\Rightarrow SNR = \left[Q^{-1}\left(\frac{BER_{M-DPSK}\ \log_2 M}{2}\right)\ \frac{1}{\sqrt{2}\ \sin\left(\frac{\pi}{M}\right)}\right]^2 \end{aligned} \tag{4.18}$$

and for $M = 2$

$$\begin{aligned} BER_{2-DPSK} &= Q\left(\sqrt{2\ SNR}\right) \\ &\Rightarrow \sqrt{2\ SNR} = Q^{-1}\left(BER\right) \\ &\Rightarrow SNR = \frac{\left[Q^{-1}\left(BER\right)\right]^2}{2} \end{aligned} \tag{4.19}$$

After these steps, the expression for the channel attenuation a_{Ch} from 4.3 can be substituted into the SNR equation 4.1, allowing for the explicit derivation of d. Since this passage has already been done in 4.2.2, we reference to the equation 4.16 and we substitute the SNRs expressions:
For $M \geq 4$

$$\begin{aligned} d &= \sqrt{\frac{P_{Tx}\ D^2\ \lambda^2}{k\ T_0\ [F-1]\ B\ (4\pi)^2\ SNR}} \Rightarrow \\ d &= \sqrt{\frac{P_{Tx}\ D^2\ \lambda^2\ 2\ \sin^2\left(\frac{\pi}{M}\right)}{k\ T_0\ [F-1]\ B\ (4\pi)^2\ \left[Q^{-1}\left(\frac{BER\ \log_2 M}{2}\right)\right]^2}} \end{aligned} \tag{4.20}$$

and we substitute B from 4.13

$$d = \sqrt{\frac{P_{Tx}\ D^2\ \lambda^2\ \sin^2\left(\frac{\pi}{M}\right)\ T_w}{k\ T_0\ [F-1]\ (1+\beta)\ (4\pi)^2\ \left[Q^{-1}\left(\frac{BER\ \log_2 M}{2}\right)\right]^2}} \tag{4.21}$$

Instead, for $M = 2$

$$d = \sqrt{\frac{P_{Tx}\ D^2\ \lambda^2}{k\ T_0\ [F-1]\ B\ (4\pi)^2\ SNR}} \Rightarrow$$
$$d = \sqrt{\frac{P_{Tx}\ D^2\ \lambda^2\ 2}{k\ T_0\ [F-1]\ B\ (4\pi)^2\ \left[Q^{-1}(BER)\right]^2}} \tag{4.22}$$

and substituting B from 4.13 gives:

$$d = \sqrt{\frac{P_{Tx}\ D^2\ \lambda^2\ T_w}{k\ T_0\ [F-1]\ (1+\beta)\ (4\pi)^2\ \left[Q^{-1}(BER)\right]^2}} \tag{4.23}$$

Thus, we can insert the numerical values from 4.2.1 to calculate the distances for each DPSK modulation scheme. The distances for different DPSK modulations are computed using the simple Matlab script reported in Appendix B, which leads to the following results:

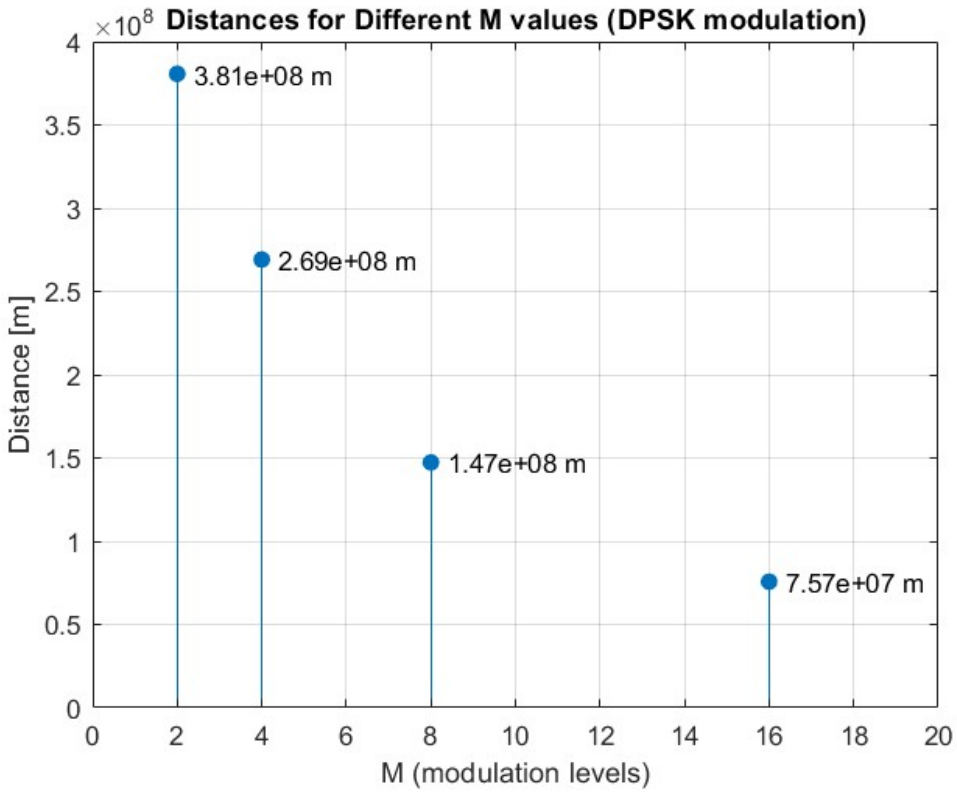

Figure 4.3: Distances related to table 4.2

Table 4.2: Distances for different M values (DPSK modulation)

M	Distance [m]	Distance [AU]
2	$3.806677 \cdot 10^8$	$2.5445705 \cdot 10^{-3}$
4	$2.691727 \cdot 10^8$	$1.799283 \cdot 10^{-3}$
8	$1.473012 \cdot 10^8$	$9.846342 \cdot 10^{-4}$
16	$7.569851 \cdot 10^7$	$5.060061 \cdot 10^{-4}$

Below is reported a graph comparing the results in terms of probes-distances obtained for both PPM and DPSK modulation scheme.

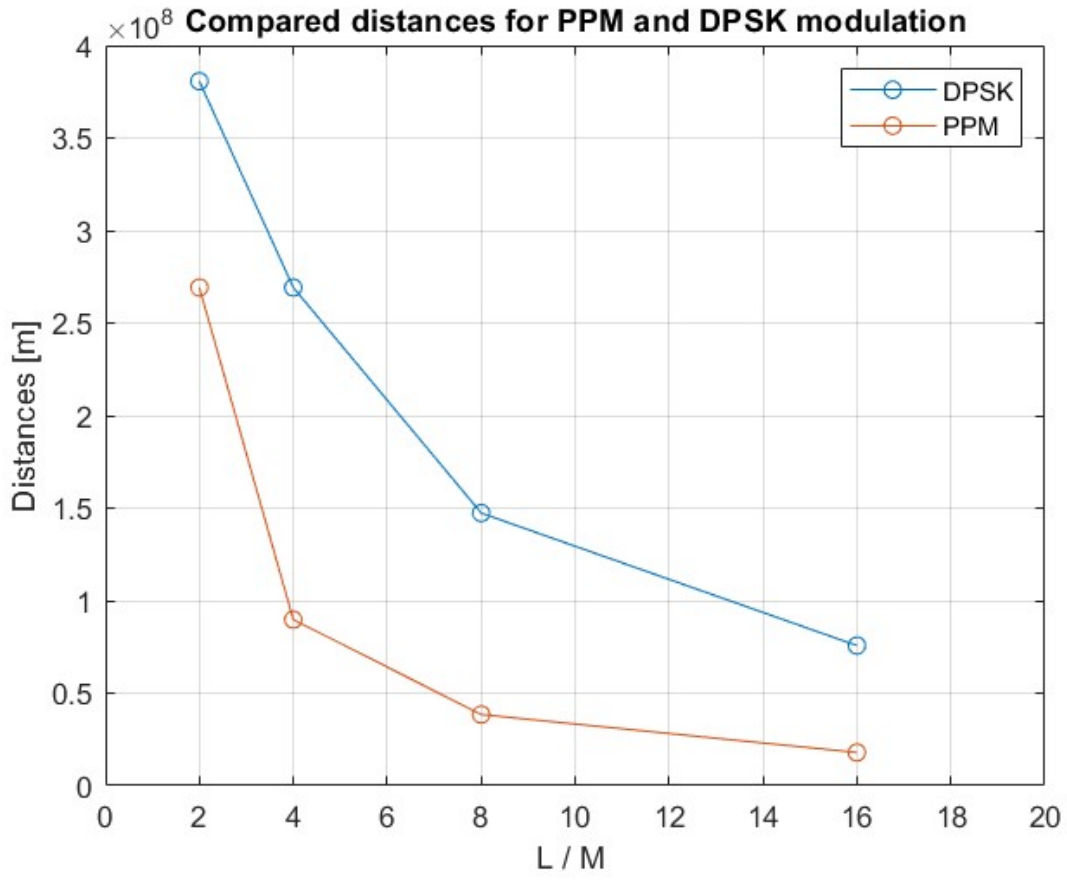

Figure 4.4: Compared distances for different modulation schemes

From the figure it is possible to note that: given a certain number of symbols (L or M) and a specific BER allowed, the DPSK modulation scheme will reach further distances than the PPM modulation.

4.3 Redundancy

With the previous computations it has been discovered the maximum distance, relating to a specific modulation, at which the probes have to be set apart so that they would be able to communicate with a specific power budget and a bit-error probability of 10^{-9}.
Given the results reported in Table 4.1 and Table 4.2, a straightforward approach could be to choose a modulation and set the probes at the maximum distance that will allow the spacecrafts to communicate.
Even though this solution could work in theory, it does not account for possible failures. Indeed, what if a probe, for any reason such as a defective communication system, or a damage in the power supply apparatus, stops working? This scenario would lead to a probe not being able to fulfil its duty in forwarding data, making useless all the probes that have been launched before the defective one.
Luckily, this setting would not cause the ineffectiveness of all the nanosatellites swarm, but it is unacceptable that because of the failure of just one probe, an undetermined percentage of the swarm would be lost. Because of this reason, multiple redundancy margins are considered so that, unfortunate scenarios like the loss of one or more probes, would not cause the uselessness of part of the swarm.

4.3.1 Modulation redundancy

A possible fault of the system could occur in the modems of the communication apparatus [5, 6]. Even if the choice of having multiple modulations schemes available was not initially taken because of redundancy reasons, the previously discussed settings in which DPSK and PPM are used, play a fundamental role in the fault tolerability of the system. As analyzed in Section 3.2.1, Section 3.2.2 and Section 4.1, two modems will be carried in the spacecraft.
Therefore, in case of a breakdown of one of the two modems, the other one would be able to keep the connection open preventing the loss of part of the swarm. Clearly, as shown in Section 4.2.2 and Section 4.2.3, a suitable choice for the distance at which the satellites are placed has to be made in order to allow the switch of the modulation scheme. Such analysis is left to the following section.

4.3.2 Distance choice

To ensure that in case of a loss of one or more probes the swarm will keep working properly, a choice in the inter-satellite distance has to be taken.
In particular, the solution that will be presented hereafter, will be based on the following constraints [43]:

1. In case of no failure, the probes will communicate with 16-PPM or 16-DPSK;

2. In case of one failure, the preceding and following probes to the faulty one will communicate with 8-PPM or 8-DPSK;

3. In case of two adjacent failed probes, the preceding and following satellites to the faulty couple will communicate with 4-PPM or 4-DPSK.

PPM case

In the case of PPM, to fulfil the constraints set on Section 4.3.2 we need to solve the following system of inequalities where d_{PPM} represents the distance between each probe and d_4, d_8, d_{16} are the distances relative to each L-PPM modulation taken from Table 4.1.

$$\begin{cases} d_{PPM} < d_{16} \\ 2d_{PPM} < d_8 \\ 3d_{PPM} < d_4 \end{cases} \Rightarrow \begin{cases} d_{PPM} < 1.794485 \cdot 10^7 \\ d_{PPM} < \dfrac{3.845325 \cdot 10^7}{2} \\ d_{PPM} < \dfrac{8.972425 \cdot 10^7}{3} \end{cases} \Rightarrow \begin{cases} d_{PPM} < 1.794485 \cdot 10^7 \text{ m} \\ d_{PPM} < 1.9226625 \cdot 10^7 \text{ m} \\ d_{PPM} < 2.9908083 \cdot 10^7 \text{ m} \end{cases}$$

Therefore, when dealing with PPM, the distance d at which the probes have to be set apart is:

$$d_{PPM} < 1.794485 \cdot 10^7 \text{ m} \tag{4.24}$$

DPSK case

With analogous reasoning as before, for DPSK modulation, to meet the constraints outlined in Section 4.3.2, we must solve the following system of inequalities. Here, d represents the distance between each probe, while d_4, d_8, and d_{16} denote the respective distances for each M-DPSK modulation as specified in Table 4.2.

$$\begin{cases} d_{DPSK} < d_{16} \\ 2d_{DPSK} < d_8 \\ 3d_{DPSK} < d_4 \end{cases} \Rightarrow \begin{cases} d_{DPSK} < 7.569851 \cdot 10^7 \\ d_{DPSK} < \dfrac{1.473012 \cdot 10^8}{2} \\ d_{DPSK} < \dfrac{2.691727 \cdot 10^8}{3} \end{cases} \Rightarrow \begin{cases} d_{DPSK} < 7.569851 \cdot 10^7 \text{ m} \\ d_{DPSK} < 7.3650600 \cdot 10^7 \text{ m} \\ d_{DPSK} < 8.9724233 \cdot 10^7 \text{ m} \end{cases}$$

Therefore, when dealing with DPSK, the distance d at which the probes have to be set apart is:

$$d_{PPM} < 7.3650600 \cdot 10^7 \text{ m} \tag{4.25}$$

In conclusion, based on the previous section's constraint, that at least one of the PPM or DPSK modulations should function in case one of the modems fails, it is crucial to set a distance d between each probe that meets this redundancy requirement. Thus, the final distance d to be adopted, as determined from prior calculations, is the minimum distances between d_{PPM} and d_{DPSK}. Therefore:

$$d < min\{d_{PPM}, d_{DPSK}\} = 1.794485 \cdot 10^7 \text{ m} \tag{4.26}$$

4.3.3 Antenna redundancy

Another system, which in case of failure can cause devastating consequences, is the laser beam emitter. A simple but very effective solution to a possible fault of the antenna is to double the number of beam emitters available on the satellite.
This solution comes from an observation of the choices that have been taken while building the LCRD satellite [5–7, 38, 39]. The basic operative setting of the LCRD is to receive data from one of its two communication systems and forward the information in real time through the other one. This solution makes the data transfer very fast and effective.
A similar approach could be taken while defining the structure of the payload that has been designed for the mission considered in this thesis. Therefore, in the case of an unfortunate failure of one of the two antennas, we could exploit the remaining one to both receive and transmit the data. In particular, the telescope would be initially pointed to the preceding probe, in order to gather the information that is being transmitted. Afterwards, once the data has been cached on a spacecraft internal memory, the antenna would be turned around and pointed to the following probe to transmit the gathered data.

This solution would be a very inefficient form of *store-and-forward* packet switching [42], but rather than losing part of the swarm, this is obviously a better choice.
It is important to note that particular attention should be paid while choosing the dimension of the memory in the probe. Let's now build an example which references Figure 4.5. Consider three probes which are part of the swarm, the first and the last ones (A and C) are working properly, while the one in the middle (B) has one of the two beam emitter that is defective.

The scenario described before will consider the following procedure: first, B points its telescope to A. Then A keeps transmitting to B as long as the memory of B has been completely filled up. Once this happens, B rotates its antenna to point it towards C and as soon as the transmitter and receiver are properly aligned, B starts to transmit the stored data to C etc.

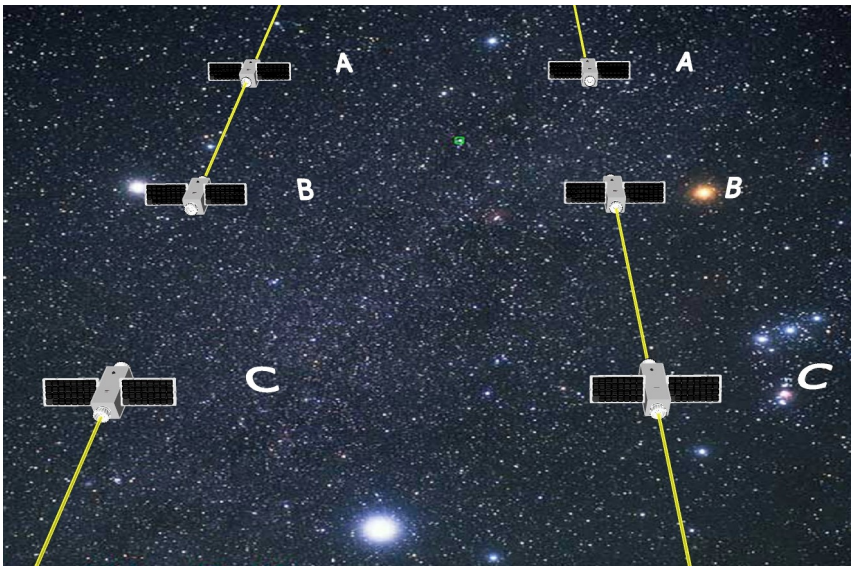

Figure 4.5: Example of *store-and-forward*

The efficiency of this solution has a clear dependence on the memory size of B. If the storage of B's memory is too small, the procedure of rotating the antenna back and forth will consume a lot of time, highly increasing the delay between the transmission and reception of the packets. On the other hand, if the memory is too big, the weight of the SSD or HDD will increase, changing the mass budget computed for the payload. To solve wisely this problem, a statistical analysis of the delay of information should be done, considering the probability of having a faulty antenna, the average time required to rotate the communication system, the mass budget available and the maximum amount of delay that is acceptable. Such statistical analysis is not part of this thesis and could be the object of future work.

Chapter 5

Future work

As this thesis was being developed, and multiple solutions to the challenges addressed were being examined, many ideas and possible projects to improve the current settings of the mission arose.
Because of the non-trivial nature of these proposals, the author does not pretend to deepen them in this current work. Anyhow, the possibility of going into details of these projects in future works is not excluded, that is because some of the previously mentioned ideas are briefly presented below.

5.1 Hierarchical swarm

Resuming the scenario studied in this work, multiple light-weight light-driven probes are launched, forming a linear topology, to explore the Solar System [3]. Each probe is equal to the others and is expected to communicate with its adjacent spacecrafts. In this scenario, even if each nanosatellite is perfectly identical to the others, providing a reduction of the per-probe cost because of the concept of *economy of scale* [50], a better approach to reduce the costs could be studied. As stated before, all the nanosatellites are designed to be identical to one another, this

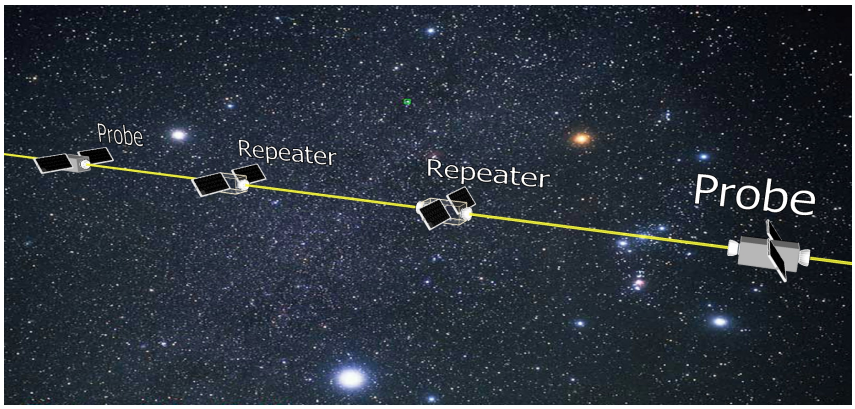

Figure 5.1: Hierarchical swarm

could expose the system to the chance of having multiple observations of the same phenomenon from the same place. Even if redundancy in the observations can be positive for some scientific research, it is possible that an observation of the same phenomena for each probe is not necessary.

Because of this reasoning, it is proposed to create two different versions of the probes: one, which is the primary probe, will be a nanosatellite of the same kind as the one presented in this thesis, capable of observing phenomena and transmitting data. On the other hand, the secondary probe will be just responsible for receiving data from the preceding probe and retransmitting the information received to the following one [42].

Even if this solution would lead to two different models of probes (very similar to one another), the savings related to a similar approach could be non-negligible. For example, a lighter probe could sensibly decrease the costs of launching the satellites into orbit [12], or, in the case of laser-driven propulsion [15], a probe weighing less will require less light power decreasing the cost of the energy consumed. Moreover, also the cost of the scientific instrumentations that will not be added to the probes will be saved.

5.2 Power hopping

As stated several times in this thesis, the amount of power available to the probes is extremely limited. Indeed, the energy source responsible for powering all the devices of the spacecraft payload is the solar panel array [30].

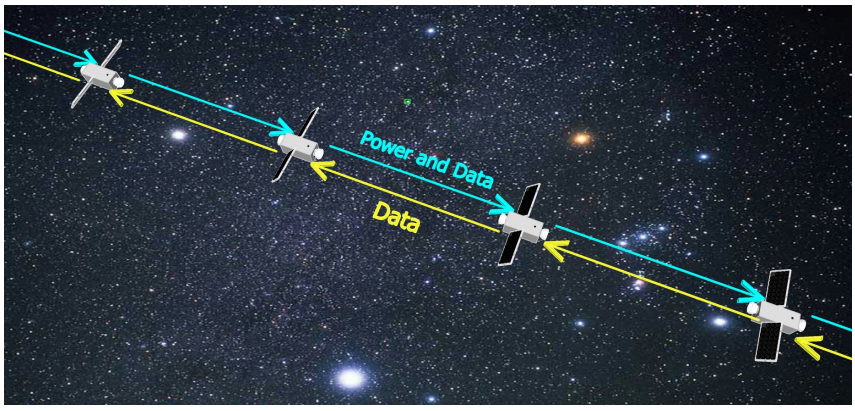

Figure 5.2: Power hopping

As stated in Section 2.2.2, the average power production of the photovoltaic system, when the probe is in the neighbourhood of Mars, is around 3 W [3]. However, because the swarm is expected to travel far beyond Mars' orbit, without a hypothetical limit because of the system scalability, the power generated from solar radiation will keep decreasing, reducing the spacecraft communication capability.

To overcome this issue, a possible solution, which should be deepened in future work, is

outlined below. The project proposed suggests the use of the communication system of each satellite to transfer energy to the following probe. As stated in [30], with the PPM or DPSK signal it is possible to transmit also a DC component, which can be then separated to the received signal and used for power harvesting. Even if this is not an efficient means to transfer power, the explained concept could be explored to power the furthest probes.

In particular, the scenario supposed is the following: on the surface of Earth, or in orbit around our planet, we assume to have available an extremely powerful laser emitter which is expected to irradiate the solar panels of the closest probe [2]. Afterwards, the mentioned probe hit by the intense laser beam, will transfer through its optical communication system, to the following probe, part of the energy received. The procedure is then repeated for each spacecraft finally transmitting part of the original power to the most distant probe. A procedure like the one just described is not very different to the transfer of information that is supposed in this thesis [42], in this scenario we just intend to parallel transfer both information and energy.
Clearly, such an approach has some criticisms: first of all a lot of power will be dispersed at each hop, also the communicating systems need to be capable of transmitting a highly biased signal and the receiver is required to handle such power.
Nevertheless, if the apparatuses in the probes were properly designed to tolerate such high power and minimize the losses, a transmission of energy like the one described above could be considered and deepened.

5.3 Lightsail assembly

The usual procedure when a ligthsail-propelled spacecraft is launched in orbit, is to pack the solar sail by folding it multiple times in order to occupy less space and decrease the chance of damage [17]. Once the probe reaches the orbit it then unfolds its lightsail and begins its journey. The procedure of unfolding a lightsail is usually risky and relies on small electrical motors. Because of the limited mass available in the studied mission [1, 3, 15, 17], it is primary to find some ways to reduce to the essential the number of components that build the spacecraft. Therefore, because of the single utilization of the motors responsible for extending the sail booms and unfolding the solarsail, it has been thought to delegate this duty to an external device.
The proposed system is an orbiting satellite which will have the task of assembling the lightsails and payloads once they have already reached the orbit. This solution, apart from the weight saving, will have multiple advantages. For example, if this external joining was not exploited, in the case of a faulty motor or a brake of the lightsail during the launch, it would be necessary to discard the entire probe causing an economic loss, or worse, a missing spacecraft in the swarm.

Instead, if an external assembling system were used, all those inconveniences could be avoided by discarding in advance the defective solarsails and circumventing possible motor fails.

Chapter 6

Conclusions

The presented thesis analysed multiple facets of the design of a space exploration mission. From the investigation of the propulsion systems available for the probes [3, 17, 16, Chemical propulsion], it has been concluded that the best choice for such a project is the use of a *propellent-less photonic thruster* [20]. The lightsails will be accelerated thanks to the momentum of the photons [18], these photons will be generated thanks to a laser emitter placed on the Earth's surface or in orbit around our planet.

The design of the probe payload is based on the CubeSat architecture [15, 24], this not only keeps the weight of the satellite limited but also exploits an already existing technology limiting the cost of brand-new innovations.

A cornerstone of the entire thesis is the examination of the communication system. For data rate purposes [8, 9] and to not fall in the range of the regulated spectrum [36], for the studied scenario an optical laser-based transmission system has been chosen. The devices involved are taken from the LCRD [5, 40, 41] and LLCD [6, 7, 37, 38] missions, again this is done to save the costs of developing a tailored technology.

Once the apparatus responsible for the telecommunications has been chosen, the parameters of the transmission and of the swarm had to be calculated. First of all, the decision made was to adopt the modulation schemes used in LCRD and LLCD projects: PPM and DPSK [5]. The first was chosen because of its power-conservative characteristics, while the second was selected because of its noise tolerance and fading endurance [8, 9, 43].

Given the modulation schemes, a detailed link budget has been carried out allowing the author to infer the distances at which the probes have to be set apart. The results are reported in Table

4.1 and Table 4.2, respectively referring to PPM and DPSK modulation.

From those results multiple redundancies were presented, these had the aim of increasing the swarm reliability and decreasing the chances of loose part of the satellites. For instance, considering the multiple levels of modulation examined (2, 4, 8, and 16), one proposed mechanism to mitigate potential failures involved setting the distances between the probes such that if one or two consecutive satellites malfunctioned, the modulation could be shifted from level 16 to level 8 or level 4, in order to maintain the functionality of the swarm.

Lastly, some possible works that could be studied in future were presented. For example, the chance of hierarchizing the swarm to decrease the costs was proposed [50], moreover, the feasibility of transmitting power alongside data to allow the furthest probes to gain sufficient energy [30], is a suggested topic that can be deepened.

To sum up, this thesis represents a contribution to the ongoing efforts of redefining the paradigms of space exploration. By harnessing the potential of lightsail technology and optical communications, we not only broaden our horizons for future deep space exploration but also set the stage for ongoing innovations that could further optimize the efficiency and reliability of interstellar travel.

Appendix A

PPM Matlab code

Hereafter is reported the Matlab code that has been used in Section 4.2.2 to compute the distances at which the probes have to be set apart in order to comply with the desired constraints related to PPM modulation.

```
% This script is used to compute the distance between each probe using PPM
P = 2;
D = (4 * pi) / (2*pi*(1 - cos(15 * 10^(-6))));
lamb = 1528.17 * 10^(-9);

Tw = 4 * 10^(-9);
k = physconst('Boltzmann');
T0 = 290;
F = 10^(3/10);
beta = 0.8;
ber = 10^(-9);

% Constant for conversion from meters to astronomical units
meters_to_AU = 1 / 1.496e11;

% Array of L values
L_values = [2, 4, 8, 16];

% Loop over each value of L and compute d
for L = L_values
    d_meters = sqrt( (P * D^2 * lamb^2 * Tw) / (k * T0 * (F-1) * (1 + beta)
    * (4 * pi)^2 * 2 * (qfuncinv(ber) * (L-1) )^2 ));
    d_AU = d_meters * meters_to_AU;
    fprintf('Distance for L=%d: %e meters, %e AU\n', L, d_meters, d_AU);
end

```

Appendix B

DPSK Matlab code

Below is the Matlab code used in Section 4.2.3 to calculate the distances at which the probes must be positioned to meet the desired constraints associated with DPSK modulation.

```
% Constants
P = 2;
lamb = 1528.17 * 10^(-9); % Wavelength in meters
Tw = 4 * 10^(-9); % Word time in seconds
k = physconst('Boltzmann'); % Boltzmann's constant
T0 = 290; % Room temperature in Kelvin
F = 10^(3/10); % Noise figure in linear scale
beta = 0.8; % Roll-off factor
ber = 10^(-9); % Bit error rate
D = (4 * pi) / (2 * pi * (1 - cos(15 * 10^(-6)))); % distance formula

% Constant for conversion from meters to astronomical units
meters_to_AU = 1 / 1.496e11;

% Values of M, including M = 2
M_values = [2, 4, 8, 16];

% Initialize arrays to store results
d_values_meters = zeros(size(M_values));
d_values_AU = zeros(size(M_values));

% Loop through each M value
for i = 1:length(M_values)
    M = M_values(i);

    if M == 2
        % Use the formula for M = 2
        d = sqrt((P * D^2 * lamb^2 * Tw) / ...
```

```
                (k * T0 * (F - 1) * (1 + beta) * (4 * pi)^2 * ...
                 (qfuncinv(ber))^2));
    else
        % Calculate distance d for the current M in meters
        d = sqrt((P * D^2 * lamb^2 * (sin(pi / M)^2) * Tw) / ...
                (k * T0 * (F - 1) * (1 + beta) * (4 * pi)^2 * ...
                 (qfuncinv((ber * log2(M)) / 2))^2));
    end

    % Store the results in meters and AU
    d_values_meters(i) = d; % Store distance in meters
    d_values_AU(i) = d * meters_to_AU; % Convert to astronomical units
end

% Set the display format to scientific for clearer readability
format longE;

% Display the results
disp('Calculated distances for M = 2, 4, 8, 16:');
disp('Distances in meters (scientific notation):');
disp(array2table(d_values_meters', 'RowNames', {'M = 2', 'M = 4', 'M = 8',
    'M = 16'}, ...
     'VariableNames', {'Distance_meters'}));
disp('Distances in astronomical units:');
disp(array2table(d_values_AU', 'RowNames', {'M = 2', 'M = 4', 'M = 8', 'M =
    16'}, ...
     'VariableNames', {'Distance_AU'}));
```

Bibliography

[1] S. G. Turyshev *et al.*, "Science opportunities with solar sailing smallsats," *Planetary and Space Science*, p. 105 744, 2023.

[2] E. Duplay, Z. F. Bao, S. R. Rosero, A. Sinha, and A. Higgins, "Design of a rapid transit to mars mission using laser-thermal propulsion," *Acta Astronautica*, vol. 192, pp. 143–156, 2022.

[3] G. Santi *et al.*, "Swarm of lightsail nanosatellites for solar system exploration," *Scientific Reports*, vol. 13, no. 1, p. 19 583, 2023.

[4] A. Poghosyan and A. Golkar, "Cubesat evolution: Analyzing cubesat capabilities for conducting science missions," *Progress in Aerospace Sciences*, vol. 88, pp. 59–83, 2017.

[5] B. Edwards, "Overview of the laser communications relay demonstration project," *SpaceOps 2012*, p. 1 261 897, 2012.

[6] M. Sans, Z. Sodnik, I. Zayer, and R. Daddato, "Design of the esa optical ground station for participation in llcd," *Proc. ICSOS*, pp. 9–12, 2012.

[7] D. M. Boroson, J. J. Scozzafava, D. V. Murphy, B. S. Robinson, and M. Lincoln, "The lunar laser communications demonstration (llcd)," in *2009 Third IEEE International Conference on Space Mission Challenges for Information Technology*, IEEE, 2009, pp. 23–28.

[8] A. F. Molisch, *Wireless communications*. John Wiley & Sons, 2012, vol. 34.

[9] M. M. Symon Haykin, *Analog digital communications*. John Wiley & Sons, vol. 2.

[10] H. Jones, "The recent large reduction in space launch cost," 48th International Conference on Environmental Systems, 2018.

[11] SpinLaunch, *Spinlaunch, una catapulta per lo spazio*, `https://aliveuniverse.today/flash-news/fisica-tecnologia/6039-spinlaunch-una-catapulta-per-lo-spazio`.

[12] SpinLaunch, *Spinlaunch cost saving*, `https://www.spinlaunch.com/orbital#p3`.

[13] SpinLaunch, *Spinlaunch*, `https://www.spinlaunch.com/`.

[14] G. Santi *et al.*, "Multilayers for directed energy accelerated lightsails," *Communications Materials*, vol. 3, no. 1, p. 16, 2022.

[15] M. Lingam, A. Hibberd, and A. M. Hein, "A light sail astrobiology precursor mission to enceladus and europa," *Acta Astronautica*, vol. 218, pp. 251–268, 2024, issn: 0094-5765. doi: https://doi.org/10.1016/j.actaastro.2024.02.040.

[16] NASA, *Nasa website*, https://www.nasa.gov/.

[17] I. Levchenko, K. Bazaka, S. Mazouffre, and S. Xu, "Prospects and physical mechanisms for photonic space propulsion," *Nature Photonics*, vol. 12, no. 11, pp. 649–657, 2018.

[18] Zotto, Lo Russo, and Sartori, *General Physics. Electromagnetism - Optics*. Esculapio Ingegneria, 2022, isbn: 9788893853156.

[19] Zotto, Lo Russo, and Sartori, *General Physics. Mechanics - Thermodynamics*. Edizioni La Dotta, 2021, isbn: 97888998648658.

[20] G. A. Landis, "Advanced solar-and laser-pushed lightsail concepts," 1999.

[21] L. N. Myrabo, T. R. Knowles, J. O. Bagford, and D. B. Seibert II, "Experimental investigation of laser-pushed light sails in a vacuum," in *High-Power Laser Ablation III*, SPIE, vol. 4065, 2000, pp. 521–532.

[22] J. S. Halekas *et al.*, "Electron heat flux in the near-sun environment," *Astronomy & Astrophysics*, vol. 650, A15, 2021.

[23] ESA, *About payload systems*, https://www.esa.int/Enabling_Support/Space_Engineering_Technology/About_Payload_Systems.

[24] C. Cappelletti, S. Battistini, and B. K. Malphrus, *Cubesat handbook: From mission design to operations*. Academic Press, 2020.

[25] N. Saeed, A. Elzanaty, H. Almorad, H. Dahrouj, T. Y. Al-Naffouri, and M.-S. Alouini, "Cubesat communications: Recent advances and future challenges," *IEEE Communications Surveys & Tutorials*, vol. 22, no. 3, pp. 1839–1862, 2020.

[26] J. Puig-Suari, C. Turner, and W. Ahlgren, "Development of the standard cubesat deployer and a cubesat class picosatellite," in *2001 IEEE aerospace conference proceedings (Cat. No. 01TH8542)*, IEEE, vol. 1, 2001, pp. 1–347.

[27] E. Oland and R. Schlanbusch, "Reaction wheel design for cubesats," in *2009 4th International Conference on Recent Advances in Space Technologies*, IEEE, 2009, pp. 778–783.

[28] J. Shields *et al.*, "Characterization of cubesat reaction wheel assemblies," *Journal of Small Satellites*, vol. 6, no. 1, pp. 565–580, 2017.

[29] V. Knap, L. K. Vestergaard, and D.-I. Stroe, "A review of battery technology in cubesats and small satellite solutions," *Energies*, vol. 13, no. 16, p. 4097, 2020.

[30] H. Kalita, L. Vance, V. Reddy, and J. Thangavelautham, "Laser communication and coordination control of spacecraft swarms," *arXiv preprint arXiv:1901.08875*, 2019.

[31] F. Santoni, F. Piergentili, S. Donati, M. Perelli, A. Negri, and M. Marino, "An innovative deployable solar panel system for cubesats," *Acta Astronautica*, vol. 95, pp. 210–217, 2014.

[32] T. McGuire, M. Hirsch, M. Parsons, S. Leake, and J. Straub, "A cubesat deployable solar panel system," in *Energy Harvesting and Storage: Materials, Devices, and Applications VII*, SPIE, vol. 9865, 2016, pp. 64–71.

[33] I. D. Sudit and R. C. Woods, "A study of the accuracy of various langmuir probe theories," *Journal of applied physics*, vol. 76, no. 8, pp. 4488–4498, 1994.

[34] D. Lee and N. Hershkowitz, "Ion collection by planar langmuir probes: Sheridan's model and its verification," *Physics of plasmas*, vol. 14, no. 3, 2007.

[35] B. J. Clement and M. D. Johnston, "The deep space network scheduling problem," 2005.

[36] D. M. Leive, "International telecommunications and international law: The regulation of the radio spectrum.," 1970.

[37] C. E. DeVoe *et al.*, "Optical overview and qualification of the llcd space terminal," in *International Conference on Space Optics—ICSO 2014*, SPIE, vol. 10563, 2017, pp. 115–123.

[38] J. W. Burnside, S. D. Conrad, A. D. Pillsbury, and C. E. DeVoe, "Design of an inertially stabilized telescope for the llcd," in *Free-Space Laser Communication Technologies XXIII*, SPIE, vol. 7923, 2011, pp. 133–140.

[39] D. M. Boroson *et al.*, "Overview and results of the lunar laser communication demonstration," in *Free-Space Laser Communication and Atmospheric Propagation XXVI*, SPIE, vol. 8971, 2014, pp. 213–223.

[40] NASA, *Laser communications relay demonstration (LCRD) overview*, `https://www.nasa.gov/directorates/stmd/tech-demo-missions-program/laser-communications-relay-demonstration-lcrd-overview/`.

[41] D. J. Israel, B. L. Edwards, J. D. Moores, S. Piazzolla, and S. Merritt, "The laser communications relay demonstration experiment program," in *Ka and Broadband Communications Conference*, 2017.

[42] J. Kurose and K. Ross, "Computer networks: A top down approach featuring the internet," *Peorsoim Addison Wesley*, 2010.

[43] N. Benvenuto and M. Zorzi, *Principles of communications Networks and Systems*. John Wiley & Sons, 2011.

[44] M. Stevens, D. Boroson, and D. Caplan, "A novel variable-rate pulse-position modulation system with near quantum limited performance," *Proc. IEEE LEOS*, vol. 1, 1999, pp. 301–302.

[45] Wikipedia, *Directivity*, `https://en.m.wikipedia.org/wiki/Directivity`.

[46] Wikipedia, *Solid angle*, `https://en.m.wikipedia.org/wiki/Solid_angle`.

[47] J. G. Proakis and M. Salehi, *Digital communications*. McGraw-hill, 2008.

[48] N. Azzam, M. H. Aly, and A. AboulSeoud, "Bandwidth and power efficiency of various ppm schemes for indoor wireless optical communications," in *2009 National Radio Science Conference*, IEEE, 2009, pp. 1–11.

[49] ESA, *Square-root raised cosine signals (srrc)*, `https://gssc.esa.int/navipedia/index.php/Square-Root_Raised_Cosine_Signals_%28SRRC%29`.

[50] Bernheim, Whinston, Cardani, and Moscati, *Microeconomia. Ediz. custom per Bocconi*. McGraw-Hill Education, 2023, isbn: 978-8838656149.

[51] L. Badia and F. Gringoli. "A game of one/two strategic friendly jammers versus a malicious strategic node." *IEEE Networking Letters*, vol. 1(1): 6–9, 2019.

[52] L. Prospero, R. Costa, and L. Badia, "Resource sharing in the Internet of things and selfish behaviors of the agents," *IEEE Transactions on Circuits and Systems II: Express Briefs*, vol. 68(12): 3488–3492, 2021.

[53] E. Gindullina and L. Badia, "Towards self-control of service rate for battery management in energy harvesting devices," Proc. *IEEE ICC Workshops*, pp. 355–360, 2017.

[54] N. Yu and F. Capasso, "Flat optics with designer metasurfaces," *Nature materials,* vol. 13(2):139–150, 2014.

[55] L. Canzian, L. Badia, and M. Zorzi, "Promoting cooperation in wireless relay networks through Stackelberg dynamic scheduling," *IEEE Transactions on Communications*, vol. 61(2): 700–711, 2012.

[56] Q. Wu and R. Zhang. "Beamforming optimization for wireless network aided by intelligent reflecting surface with discrete phase shifts," *IEEE Transactions on Communications*, vol. 68(3): 1838–1851, 2019.

[57] L. Badia. "A Markov analysis of selective repeat ARQ with variable round trip time," *IEEE Commun. Lett.*, vol. 17(11): 2184–2187, 2013.

[58] O. Kundacina, M. Petkovic, A. Munari, D. Vukobratovic, and L. Badia, “Move away from me! User repulsion under proximity-induced interference in OWC systems,” In *European Wireless,* pp. 308-313, VDE, 2023.

[59] Ana Díaz-Rubio, Viktar S Asadchy, Amr Elsakka, and Sergei A Tretyakov, “From the generalized reflection law to the realization of perfect anomalous reflectors,” *Science advances*, 3(8): e1602714, 2017.

[60] L. Badia, P. Casari, M. Levorato, and M. Zorzi, “Analysis of an automatic repeat request scheme addressing long delay channels,” *Proc. IEEE WAINA*, pp. 1142–1147, 2009.

[61] L. Badia, M. Levorato, and M. Zorzi, “A channel representation method for the study of hybrid retransmission-based error control,” *IEEE Transactions on Communications*, vol. 57(7), pp. 1959–1971, 2009.

[62] L. Badia, M. Rossi, M. Zorzi, “Some results on the statistics of delay terms in SR ARQ on Markov channels,” *Proc. IEEE ISWCS*, pp. 64–68, 2005.

[63] D. Kudathanthirige, D. Gunasinghe, and G. Amarasuriya, “Performance analysis of intelligent reflective surfaces for wireless communication,” In *International Conference on Communications (ICC)*: pp. 1–6, 2020.

[64] L. Badia, V. Mancuso, and M. Ajmone Marsan, “Adversarial obstruction of Millimeter Wave links,” In Mediterranean Communication and Computer Networking Conference (MedComNet), pp. 101-110, IEEE, 2023.

[65] F. Guidolin, L. Badia, and M. Zorzi, “A distributed clustering algorithm for coordinated multipoint in LTE networks”, *IEEE Wireless Communications Letters*, vol. 3(5), pp. 517–520, 2014.

[66] M. Lopez-Martinez, J. J. Alcaraz, L. Badia, and M. Zorzi, “A superprocess with upper confidence bounds for cooperative spectrum sharing” *IEEE Transactions on Mobile Computing*, vol. 15, no. 12, pp. 2939–2953, 2016.

[67] E. G. Larsson and E. A. Jorswieck, “Competition versus collaboration on the MISO interference channel,” *IEEE J. Sel. Areas Commun*., vol. 26, no. 7, pp. 1059-1069, 2008.